



## An efficient and novel way to synthesis of highly active BiVO<sub>4</sub> using homogenous precipitation

Ahmed Helal,<sup>1, 2, \*</sup>, S A El-Hakam<sup>1</sup>, S E Samra,<sup>1</sup> S M El-Sheikh,<sup>2</sup> Alaa I. Eid<sup>3</sup> Jianqiang Yu<sup>4</sup>

<sup>1</sup> Department of Chemistry, Faculty of Science, Mansoura University, Mansoura, Egypt.

<sup>2</sup> Nanostructured Materials and Nanotechnology Division, Central Metallurgical Research and Development. Institute (CMRDI), P. O. 87 Helwan, Cairo 11421, Egypt.

<sup>3</sup> Composite Materials Division, Central Metallurgical Research and Development. Institute (CMRDI).

<sup>4</sup> Institute of Green Chemistry & Industrial Catalysis, School of Chemistry and Chemical Engineering, Qingdao University, Qingdao 266071, China.

Received: 14/11/2018  
Accepted: 24/12/2018

**Abstract:** The improvement of the photocatalyst performance with reducing both equipment and cost of its production still the most important concern for finding, 1) Required material properties, 2) Possibility of manufactured mass production from the photocatalyst. Now, we reveal, a novel way for synthesis of BiVO<sub>4</sub> photocatalyst by homogenous precipitation. Different surfactants were adding to assist in the orientation. XRD, SEM, Raman, and DRS were used to evaluate construction of the as-synthesized BiVO<sub>4</sub> photocatalysts. The performance of photocatalytic efficiency of the as-synthesized catalysts were estimated by photoelectrochemical tests and photodegradation of Methylene blue (MB) dye as wastewater module.

**Keywords:** BiVO<sub>4</sub>; Photocatalyst; MB photodegradation; Homogenous precipitation

### 1.Introduction:

Bismuth vanadate (BiVO<sub>4</sub>) show interesting physicochemical properties including ferroelasticity, ionic conductivity, acousto-optical photocatalytic activity [1, 2]. So, it has been recently introduced into the gas sensors devices, posistors, solid-state electrolytes, lithium batteries and non-hazardous yellow pigment for high performance lead-free paints [3]. Also, it is an excellent material in the field of visible light driven photocatalysts [4–7]. BiVO<sub>4</sub> exists in three polymorphs, monoclinic scheelite, tetragonal zircon, and tetragonal scheelite. The monoclinic scheelite construction being the most reactive phase with its direct band gap of ~2.4-2.5 eV at ambient temperature [8, 9]. Nevertheless, the pure monoclinic BiVO<sub>4</sub> was still has low activity in the visible-light range [10], due to highly recombination, diminutive lifetime of photogenerated Electron-hole pairs, low electrical conductivity, slow hole transfer kinetics for water oxidation [11]. The activity

of BiVO<sub>4</sub> is powerfully associated to its crystallinity and morphology [9]. Numerous techniques have been described to synthesized BiVO<sub>4</sub> in both bulk and thin film. For example, solid-state reaction [12], aqueous solution method [13], co-precipitation [14], solvothermal [15], molten salt method [16], Microwave irradiation [17], and Metal organic decomposition [18], have been used to prepare BiVO<sub>4</sub> with different shapes. In the ordinary precipitation process, the metal oxide was produced during addition ammonia directly to metal cation solution. This technique gives a slightly controlled to the shape and size of precipitated particles due to the rapid rise of solution pH and concentration of the metal oxide [19]. There is another method called homogeneous precipitation. The important feature of this technique is the a greatly uniform precipitation which carried out by a rise in the pH of the reaction mixture and this homogeneity achieved by thermal decay of

urea. This occurred when urea has been dissolved into an acidic media of a metal source and heated to about 90°C, the urea decays gradually due to ejection of ammonia and carbonate ions into the acid media. These procedures produced a regular and uniform nucleation and uniformly particles of insoluble BiVO<sub>4</sub> samples [20]. The homogeneous precipitation process was used previously to synthesize TiO<sub>2</sub> [21], Al<sub>2</sub>O<sub>3</sub> [22], MgAl<sub>2</sub>O<sub>4</sub> [23], Fe<sub>3</sub>O<sub>4</sub> [24], and Fe(OH)<sub>2</sub> [25]. In this study, we report homogeneous precipitation as novel assemble of monoclinic BiVO<sub>4</sub>.

## 1. Experimental part

### 1.1. Materials

Bismuth (III) Nitrate pentahydrate Bi(NO<sub>3</sub>)<sub>3</sub>·5H<sub>2</sub>O, Ammonium metavanadate NH<sub>4</sub>VO<sub>3</sub> were used as source for Bi and V, respectively, Polyvinylpyrrolidone (PVP), Ethylene glycol (Eg), cetyltrimethylammonium bromide (CETAB), Sodium Dodecyl Benzene Sulphonate (SDBS) were used as orienting agent and Urea has been employed as precipitating agent. MB has been used as wastewater module to evaluate photocatalytic activity the existed photocatalysts. All compounds in our work were analytical grade reagents and they were obtained from Sinopharm Chemical Reagent Co., Ltd.

### 1.1. Homogenous Precipitation of BiVO<sub>4</sub>

Firstly, Solution A: 0.24 mol/L (Bi(NO<sub>3</sub>)<sub>3</sub>·5H<sub>2</sub>O) in 100 ml of 2M nitric acid (HNO<sub>3</sub>) and solution B: 0.24 mol/L (NH<sub>4</sub>VO<sub>3</sub>) in 100 ml of 2M nitric acid (HNO<sub>3</sub>) were prepared. After completely dissolving of the precursor and mixed solution A and B together with stirring for 30 min, yellow solution was obtained. Then surfactants were used as orienting agent. After each surfactant dissolved the mixture transfer to the round flask with 0.3M of urea to complete the precipitation and neutralized the reaction mixture.

### 2.3. Characterization of the BiVO<sub>4</sub> photocatalysts.

X-ray diffraction (XRD) shapes were verified on a Bruker D8-advance x-ray diffractometer using Cu K $\alpha$  radiation  $\lambda = 0.15478$  nm, 40kv, 30mA. All results were measured at a 2 $\theta$  range between 10° and 80. The morphologies and microstructures of as-

synthesized samples were observed with scanning electron microscopy (JSM-6390LV). The Raman pattern were measured by a microprobe Raman (Thermo scientific, DXR 532 laser) device, and the excitation wavelength was at 532 nm. The spectra of the produced samples were measured on a doubled-beam UV-vis spectrophotometer (JASCO V 750) equipped with an integrating sphere. The UV-vis spectra were performed in the diffuse reflectance mode (R) and tuned to the Kubelka-Munk function F(R) to isolated the amount of light absorption from scattering. Furthermore, the band gap of prepared samples were estimated from the curve of the modified Kubelka-Munk function (F(R)E<sup>2</sup>) against the absorbed light energy E, during to the subsequent equation [26].

$$F(R) E^2 = \left( \frac{(1-R)^2}{2R} \times h\nu \right)^2 \quad (1)$$

Spectrofluorophotometer, (RF-5301 PC, Japan, SHIMADZU, 400 W, 50/60 Hz) was used to measure the photoluminescence (PL) of the produced samples with 365nm as excitation wavelength.

### 2.3. Photocatalytic efficiency and photoelectrochemical performance

The investigation of photocatalytic activity was carried out by irradiation of the MB dye include BiVO<sub>4</sub> photocatalysts using XPA-7 type photochemical reactor (Xujiang Machine Factory, Nanjing, China) attached by a 800 W Xenon lamp with a 420 nm cut-off filter. The light intensity on each quartz tube equal 12.7 mW/cm. A water-cooling circulation system was established to preserve a constant reaction temperature. 0.04g of our photocatalysts was blended with 40 ml MB [1 g/L] solution in a quartz reactor. Before the photocatalytic degradation, the solution was incubated under stirring and far from the light at room temperature for 60 min to neglect the amount of adsorption dye. The MB absorbance after complete adsorption was recorded to be the original concentration (C<sub>0</sub>). The degraded day calculated by withdrawn at regular samples at interval times (C<sub>i</sub>) from the upper part of the photoreactor. 2 mL of the reaction solution were taking at interval time followed by filtration through nylon syringe filters. The remaining concentration of samples were

measured immediately after separation using a MAPADA spectrophotometer. The photocatalytic efficiency of produced samples for photodegradation of dye was calculated by equation no 2:

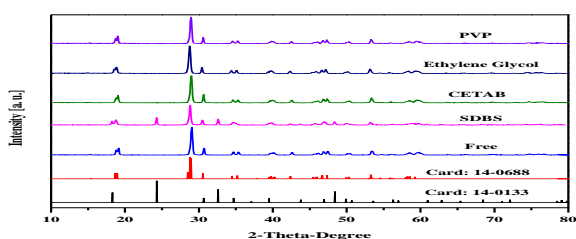
$$\% \text{ photocatalytic activity} = (1 - C_t) / C_0 \times 100 \quad (2)$$

The photoelectrochemical properties of as-prepared samples were estimated by an electrochemical workstation (CHI760E, Chenhua Instruments) with a typical three-electrode system. The samples coated on Fluorine-doped tin oxide (FTO) were used as working electrode, the other electrodes which used during measurement were Pt slice ( $2.0 \times 2.0$  cm) as counter electrode and saturated Ag/AgCl electrode were employed as reference electrode, separately. Typically, 40 mg of sample was sonicated into 1 mL of Triton X-100 mixing with 1 mL acetylacetone and 1ml Ethyl alcohol under to obtain slurry, followed by further spread onto FTO with Dimensions  $1.0 \times 1.0$  cm. The prepared photoanodes were fixed at  $200^\circ\text{C}$  for 2 h.  $0.5 \text{ M Na}_2\text{SO}_4$  and  $0.1 \text{ M Na}_2\text{SO}_3$  mixture solutions were exploit as the electrolyte media. The 500 W Xenon lamp with a 420 nm cut-off filter was used for visible light source.

### 3.Result and dissection

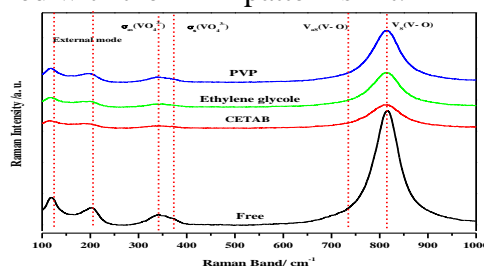
#### 3.1. Crystal structure

Figure 1, displays the XRD results of  $\text{BiVO}_4$  surfactant free,  $\text{BiVO}_4$  with SDBS,  $\text{BiVO}_4$  with CETAB,  $\text{BiVO}_4$  with Ethylene glycol and  $\text{BiVO}_4$  growth with PVP. The XRD results of produced samples exhibit a diffraction peaks defined as monoclinic  $\text{BiVO}_4$  (JCPDS card No. 14-0688). Excepting, SDBS- assisted  $\text{BiVO}_4$  shows diffraction peak indexed as mixed phase from monoclinic and tetragonal phase (JCPDS card No. 14-0133), it didn't detect any unreacted material such as  $\text{Bi}_2\text{O}_3$  or other organic compounds related to surfactant.



**Fig 1:** XRD patterns of  $\text{BiVO}_4$  photocatalysts prepared with different

These results designated that the residual surfactant removed without calcination. Also, it can notice that the  $2\theta$  peak positions of a diffraction peaks for the produced samples are shifted in each case. For example, the location of (121) and (040) reflection in Ethylene glycol assisted  $\text{BiVO}_4$  and PVP assisted  $\text{BiVO}_4$  exposed an apparent change to lower angle comparing to the sample without surfactant, indicating that the using ethylene glycol and PVP as surfactant made a great influence on the crystallization faced of  $\text{BiVO}_4$  during the homogenous precipitation technique. This impact may be due to the different molecule structures of each surfactant. Moreover, the diffraction peak at  $2\theta = 19^\circ$  show more splitting with PVP assisted  $\text{BiVO}_4$  sample which indicating the enhancement of the monoclinic crystallization phase [27]. The difference between the  $\text{BiVO}_4$  samples at different surfactants possible to be detected by Raman technique which revealed the structural information. The Raman bands in the range between  $100\text{--}1000 \text{ cm}^{-1}$  of  $\text{BiVO}_4$  produced samples were shown in Figure 2, As we seen that the position of the band near  $815 \text{ cm}^{-1}$  an obvious shift to the lower wavenumber, from 815.87, 814.90, 812.97, and 810.08 for surfactant free, PVP, Ethylene glycol, and CTAB respectively. This attributed to different degrees of imbalance in V–O length of symmetry of  $\text{VO}_4$  tetrahedral [28]. This result is matched with the XRD pattern shift.



**Fig 2:** Raman Spectra of  $\text{BiVO}_4$  sample fabricated using various

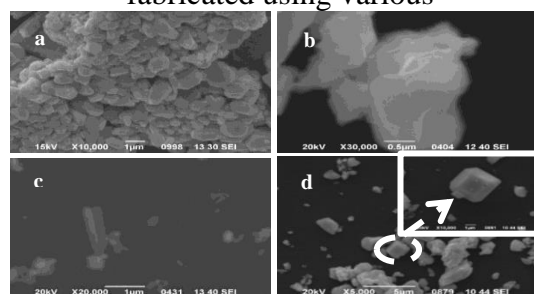


**Fig 3:** SEM images for morphology of  $\text{BiVO}_4$  sample fabricated with various surfactants.

SEM images of the synthesized  $\text{BiVO}_4$  samples with different type of surfactants are depicted in Figure. 3. It can be seen from Figure 3a that the no-surfactant-assisted  $\text{BiVO}_4$  consisted of irregular polyhedral microcrystal. with random size distributions. After Ethylene glycol is added to the reaction mixture, the typical products consist of stacked plates Figure 3b. the presence of CTAB change the morphology to irregular rods Figure. 3c, while the presence of PVP finds a new form of crystal which appeared at Figure 3d and magnified as inset figure. this form called *Truncated Bipyramid* like shape which exhibited crystal with different exposed facets and relatively sharp edges and smooth surface.

### 3.2. Optical properties, Charge Separation at different surfactant

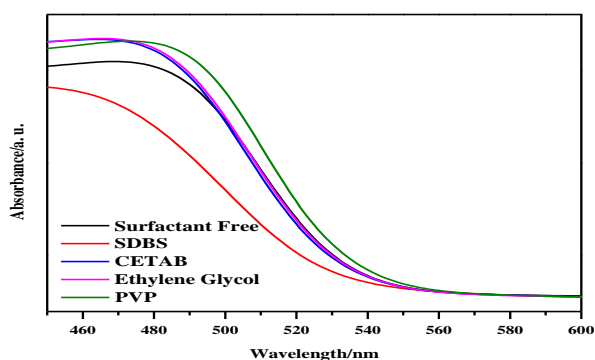


**Fig 4:**DRS spectra of  $\text{BiVO}_4$  samples with different type of surfactant.

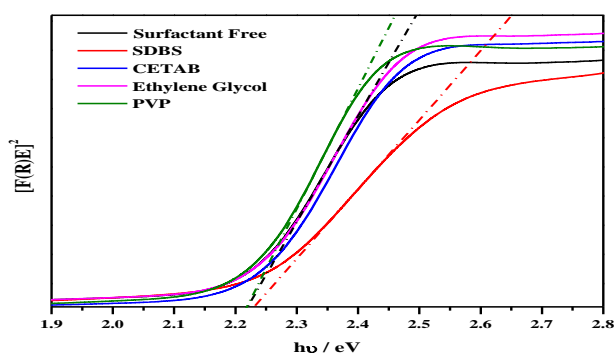


**Fig 5:**Plot of transferred Kubelka–Munk vs. energy of the light absorbed

The UV–vis DRS of samples with different type of surfactant displayed in Figure 4 revealed a various absorption shift of wavelength in addition to that of strong absorption in the UV-light region. It was found that  $\text{BiVO}_4$  sample prepared with SDBS surfactant shows absorbance less than other samples due to the ratio of tetragonal phase which appeared in the XRD [29]. The band gap

(Eg) of synthesized samples have been evaluated from the curve of the modified Kubelka-Munk function  $[F(R)E]^2$  against the energy of the absorbed light E [30] as defined in Figure 5, and was found that sample of PVP - assisted  $\text{BiVO}_4$  showed the minimum band gap which indicate that this sample has the lower bandgap level, which will enhance the photoactivity distinctive in visible light. To focus on the electronic structure, electron-hole separation process and the influence of surfactant to improve the electron-hole recombination into  $\text{BiVO}_4$  crystal, Mott Schottky (MS) and electrochemical impedance spectroscopy (EIS) curves of synthesized samples were performed. MS curves of  $\text{BiVO}_4$  samples display positive slopes as predictable for n-type semiconductors Figure 6. The flat band potential (intercept on x axis) is positively shifted after adding the surfactants, which is attributed to the swelling of band pinning of the Fermi energy edge [31]. On the other hand, the a markedly shallower slope for  $\text{BiVO}_4$  samples assisted by surfactants implying an increase of carrier densities indicating enhanced electronic conductivity [32].

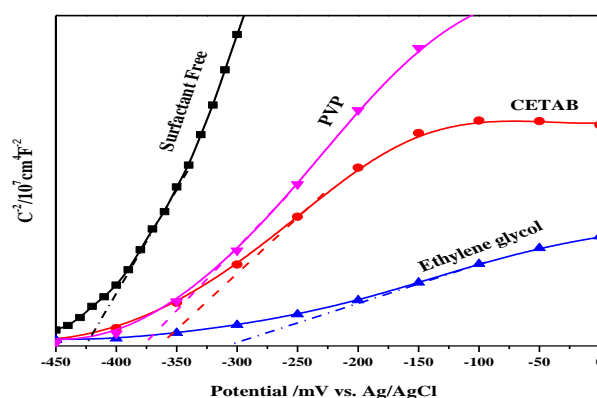


**Fig 6:**Variation of capacitance (C) with the applied potential in presented in the Mott-Schottky relationship for the  $\text{BiVO}_4$  samples with different surfactant.

Moreover, Figure 7, exposed that the electrochemical impedance spectroscopy (EIS) plot giving due to the corresponding circuit model (inset in Figure 7), where  $R_s$  and  $R_{ct}$  were denoted to the series resistance and interfacial charge transfer resistance, respectively [31]. The value of  $R_s$  for all samples were neglected, due to the similarity of the series resistance effect. After adding

the surfactant,  $R_{ct}$  decreased significantly specially in PVP assisted  $\text{BiVO}_4$ , indicating that presence of PVP greatly enhances charge transfer, these results approve that the presence of surfactant specially PVP show better electron-hole separation and electron transport property [33].

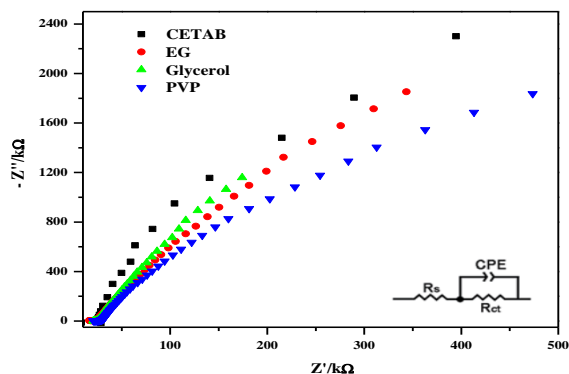


**Fig 7:** Electrochemical impedance spectra of the  $\text{BiVO}_4$  samples electrolyte. The equivalent circuit (inset).

### 3.3. Photocatalytic activity of $\text{BiVO}_4$ samples at different surfactant

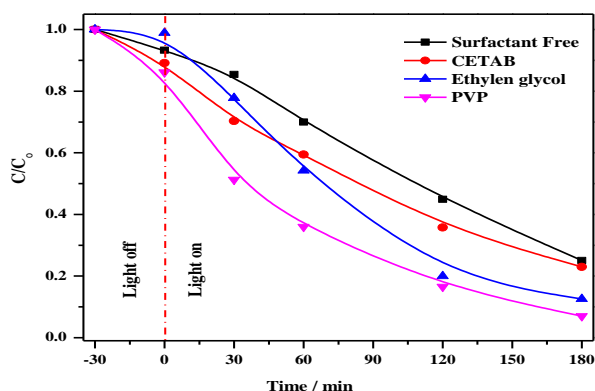


**Fig 8:** Photodegradation efficiencies of MB as a function of irradiation time for different photocatalysts.

The photocatalytic performances of crystalline  $\text{BiVO}_4$  samples synthesized with different surfactant are examined in terms of the photodegradation of MB. Figure 8, revealed the reduction in concentration of MB by  $\text{BiVO}_4$  catalysts as a function of visible irradiation time. It is clear that the photocatalytic efficiency of the  $\text{BiVO}_4$  samples treated with various surfactant much higher than that of  $\text{BiVO}_4$  synthesized without surfactant. Compared with the photodegradation of 70% of surfactant free- $\text{BiVO}_4$ , the ratio of photodegradation with PVP assisted  $\text{BiVO}_4$  powder is up to 95% in 180 min under visible-light irradiation.

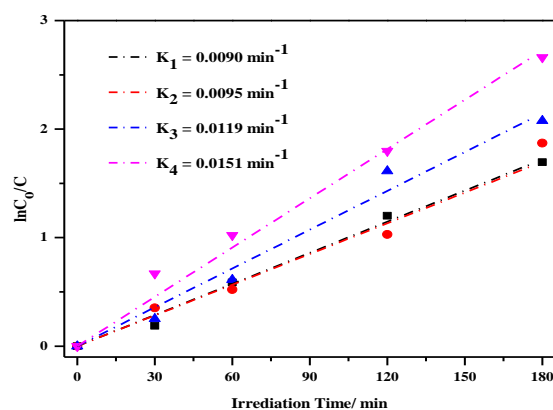


**Fig 9:** MB photodegradation kinetics curves by  $\text{BiVO}_4$  samples prepared with  $K_1$ : Surfactant Free,  $K_2$ : CETAB,  $K_3$ : Ethylene glycol,  $K_4$ : PVP

Moreover, the reaction rate constant  $k$  Figure 9, confirms the photocatalytic activity results. The PVP- assisted  $\text{BiVO}_4$  show the highest rate of reaction ( $K_4=0.0151 \text{ min}^{-1}$ ) which highest one time and half than surfactant free  $\text{BiVO}_4$  sample the photocatalytic activity of PVP- assisted  $\text{BiVO}_4$  sample may be ascribed to the *Truncated Bipyramid* like shape which appeared different facets with different activity. This shape shows diminishes in the electrons and holes recombination, and enhanced the carrier density and then, enhanced efficiency of the catalytic activity. So, we should study the increasing in concentration of PVP and impact it on the catalytic activity.

### 4. Conclusion

In Summary, we have successfully prepared for the first-time m-s  $\text{BiVO}_4$  photocatalyst via simple homogenous precipitation assisted by different surfactants as orienting agent. The characterization and photocatalytic experimental demonstrate that the increasing of the presence of PVP surfactant as orienting agent show the best results due to the formation of *Truncated Bipyramid* like shape which appeared different facets with different activity

### Acknowledgement:

This work is financially supported by the Talented Young Scientist Program, Chinese Science and Technology; National Natural Science Foundation of China for Youths (No. 21407065, 21506079), Natural Science Foundation of Shandong Province (No. ZR2016BM08).

## References

- 1 Z. Zhao, W. Luo, Z. Li, and Z. Zou, (2010). "Density functional theory study of doping effects in monoclinic clinobisvanite  $\text{BiVO}_4$ ," *Physics Letters, Section A: General, Atomic and Solid State Physics*, vol. **374**, no. 48, pp. 4919–4927,
- 2 S. Kohtani *et al.*, (2003). "Photodegradation of 4-alkylphenols using  $\text{BiVO}_4$  photocatalyst under irradiation with visible light from a solar simulator," *Applied Catalysis B: Environmental*, vol. **46**, no. 3, pp. 573–586,
- 3 K. Shantha and K. B. R. Varma, (1999) "Preparation and characterization of nanocrystalline powders of bismuth vanadate," *Materials Science and Engineering B: Solid-State Materials for Advanced Technology*, vol. **60**, no. 1, pp. 66–75,.
- 4 K. Sayama, A. Nomura, Z. Zou, R. Abe, Y. Abe, and H. Arakawa, (2003.) "Photoelectrochemical decomposition of water on nanocrystalline  $\text{BiVO}_4$  film electrodes under visible light," *Chemical Communications*, no. **23**, p. 2908,
- 5 M. Long, W. Cai, and H. Kisch, (2008). "Visible light induced photoelectrochemical properties of n- $\text{BiVO}_4$  and n- $\text{BiVO}_4$ /p- $\text{Co}_3\text{O}_4$ ," *Journal of Physical Chemistry C*, vol. **112**, no. 2, pp. 548–554,
- 6 H. Luo, A. H. Mueller, T. M. McCleskey, A. K. Burrell, E. Bauer, and Q. X. Jia, (2008) "Structural and Photoelectrochemical Properties of  $\text{BiVO}_4$  Thin Films," *The Journal of Physical Chemistry C*, vol. **112**, no. 15, pp. 6099–6102,.
- 7 K. Sayama *et al.*, (2006). "Photoelectrochemical decomposition of water into  $\text{H}_2$  and  $\text{O}_2$  on porous  $\text{BiVO}_4$  thin-film electrodes under visible light and significant effect of Ag Ion treatment," *Journal of Physical Chemistry B*, vol. **110**, no. 23, pp. 11352–11360,
- 8 A. Kudo, K. Omori, and H. Kato, (1999). "A novel aqueous process for preparation of crystal form-controlled and highly crystalline  $\text{BiVO}_4$  powder from layered vanadates at room temperature and its photocatalytic and photophysical properties," *Journal of the American Chemical Society*, vol. **121**, no. 49, pp. 11459–11467,
- 9 S. Tokunaga, H. Kato, and A. Kudo, (2001.) "Selective preparation of monoclinic and tetragonal  $\text{BiVO}_4$  with scheelite structure and their photocatalytic properties," *Chemistry of Materials*, vol. **13**, no. 12, pp. 4624–4628,
- 10 X. Yan, W. Li, A. G. Aberle, and S. Venkataraj, (2015) "Surface texturing studies of bilayer transparent conductive oxide (TCO) structures as front electrode for thin-film silicon solar cells," *Journal of Materials Science: Materials in Electronics*, vol. **26**, no. 9, pp. 7049–7058,
- 11 M. Long, W. Cai, J. Cai, B. Zhou, X. Chai, and Y. Wu, (2006.) "Efficient Photocatalytic Degradation of Phenol over  $\text{Co}_3\text{O}_4/\text{BiVO}_4$  Composite under Visible Light Irradiation," *The Journal of Physical Chemistry B*, vol. **110**, no. 41, pp. 20211–20216,
- 12 D. K. Zhong, S. Choi, and D. R. Gamelin, (2011) "Near-complete suppression of surface recombination in solar photoelectrolysis by 'co-Pi' catalyst-modified  $\text{W}:\text{BiVO}_4$ ," *Journal of the American Chemical Society*, vol. **133**, no. 45, pp. 18370–18377,.
- 13 S. K. Pilli, T. E. Furtak, L. D. Brown, T. G. Deutsch, J. A. Turner, and A. M. Herring, (2011.) "Cobalt-phosphate (Co-Pi) catalyst modified Mo-doped  $\text{BiVO}_4$  photoelectrodes for solar water oxidation," *Energy and Environmental Science*, vol. **4**, no. 12, pp. 5028–5034,
- 14 Y. X. Song Baia, (2010). "Some recent developments in surface and interface design for photocatalytic and electrocatalytic hybrid structures," *Optoelectronics and Advanced Materials, Rapid Communications*, vol. **4**, no. 8, pp. 1166–1169,
- 15 D. Wu *et al.*, (2016.) "Visible-light-driven photocatalytic bacterial inactivation and the mechanism of zinc oxysulfide under LED light irradiation," *Journal of Materials Chemistry A*, vol. **4**, no. 3, pp. 1052–1059,
- 16 Y. Liu *et al.*, (2010). "Low-temperature synthesis of  $\text{BiVO}_4$  crystallites in molten salt medium and their UV-vis absorption," *Ceramics International*, vol. **36**, no. 7, pp. 2073–2077,
- 17 H. M. Zhang, J. B. Liu, H. Wang, W. X. Zhang, and H. Yan, (2008). "Rapid microwave-assisted synthesis of phase controlled  $\text{BiVO}_4$  nanocrystals and research on photocatalytic properties under visible light irradiation," *Journal of Nanoparticle Research*, vol. **10**, no. 5, pp. 767–774,
- 18 A. Galembeck and O. L. Alves, (2002). "Bismuth vanadate synthesis by metallo-organic decomposition: Thermal decomposition study and particle size control," *Journal of Materials Science*, vol. **37**, no. 10, pp. 1923–1927,
- 19 H. Fan *et al.*, (2011) "Hydrothermal synthesis and photoelectric properties of  $\text{BiVO}_4$  with different morphologies: An efficient visible-light photocatalyst," *Applied Surface Science*,

- vol. **257**, no. 17, pp. 7758–7762,.
- 20 P. Pookmanee, S. Kojinok, and S. Phanichphant, (2012). “Bismuth vanadate ( $\text{BiVO}_4$ ) powder prepared by the sol-gel method,” *Journal of Metals, Materials and Minerals*, vol. **22**, no. 2, pp. 49–53,
  - 21 D. S. Seo and H. Kim, (2003.) “Synthesis and characterization of  $\text{TiO}_2$  nanocrystalline powder prepared by homogeneous precipitation using urea,” *J. Mater. Res.*, vol. **18**, no. 3, pp. 571–577,
  - 22 I. Yasui, (1988) “Synthesis of hydrous  $\text{SnO}_2$  and  $\text{SnO}_2$ -coated  $\text{TiO}_2$  powders by the homogeneous precipitation method and their characterization,” *JOURNAL OF MATERIALS SCIENCE*, vol. **23**, pp. 637–642,.
  - 23 F. Meshkani and S. Fateme, (2017.) “Nickel catalyst supported on mesoporous  $\text{MgAl}_2\text{O}_4$  nanopowders synthesized via a homogenous precipitation method for dry reforming reaction,” *Research on Chemical Intermediates*, vol. **43**, pp. 545–559,
  - 24 J. Chen, Y. Qian, and X. Wei, (2010) “Comparison of magnetic-nanometer titanium dioxide / ferriferous oxide ( $\text{TiO}_2 / \text{Fe}_3\text{O}_4$ ) composite photocatalyst prepared by acid – sol and homogeneous precipitation methods,” *J Mater Sci*, no. mild, pp. 6018–6024,.
  - 25 J. P. L. D. B. DOUSMA, (1976). “Hydrolysis-Precipitation Studies of Iron Solutions,” *Colloid and Interface Science*, vol. **56**, no. 3,
  - 26 A. Helal, F. A. Harraz, A. A. Ismail, T. M. Sami, and I. A. Ibrahim, (2016). “Controlled synthesis of bismuth sulfide nanorods by hydrothermal method and their photocatalytic activity,” *Materials and Design*, vol. **102**, pp. 202–212,
  - 27 Z. Zhu, L. Zhang, J. Li, J. Du, Y. Zhang, and J. Zhou, (2013) “Synthesis and photocatalytic behavior of  $\text{BiVO}_4$  with decahedral structure,” *Ceramics International*, vol. **39**, no. 7, pp. 7461–7465,
  - 28 S. R. M. Thalluri, C. Martinez-Suarez, A. Virga, N. Russo, and G. Saracco, (2013). “Insights from Crystal Size and Band Gap on the Catalytic Activity of Monoclinic  $\text{BiVO}_4$ ,” *International Journal of Chemical Engineering and Applications*, vol. **4**, no. 5, pp. 305–309,
  - 29 H. Fu, C. Pan, W. Yao, and Y. Zhu, (2005) “Visible-light-induced degradation of rhodamine B by nanosized  $\text{Bi}_2\text{WO}_6$ ,” *Journal of Physical Chemistry B*, vol. **109**, no. 47, pp. 22432–22439,.
  - 30 A. V. J. TAUC, R. GRIGOROVICI, (1966), “Optical Properties and Electronic Structure of Amorphous Germanium,” in *Physica Status Solidi (B)*, vol. **15**, no. 2, pp. 627–637.
  - 31 X. Lv *et al.*, (2017.) “ $\text{Fe}_2\text{TiO}_5$ -incorporated hematite with surface P-modification for high-efficiency solar water splitting,” *Nano Energy*, vol. **32**, pp. 526–532,
  - 32 Y. Wang *et al.*, (2013) “Simultaneous Etching and Doping of  $\text{TiO}_2$  Nanowire Arrays for Enhanced Photoelectrochemical Performance,” *ACS Nano*, vol. **7**, no. 10, pp. 9375–9383,.
  - 33 C. Mao, F. Zuo, Y. Hou, X. Bu, and P. Feng, 2014. “In Situ Preparation of a  $\text{Ti}^{3+}$  Self-Doped  $\text{TiO}_2$  Film with Enhanced Activity as Photoanode by  $\text{N}_2\text{H}_4$  Reduction,” *Angewandte Chemie International Edition*, vol. **53**, no. 39, pp. 10485–10489,